eprints@whiterose.ac.uk
https://eprints.whiterose.ac.uk/

Improving the surface characteristics of Ti-6Al-4V and Timetal 834 using PIRAC nitriding treatments

B. Attard [a], A. Leyland [b], A. Matthews [c], E. Y. Gutmanas [d], I. Gotman [d], G. Cassar [a, *]

[a] Department of Metallurgy and Materials Engineering, University of Malta, Msida, MSD2080, Malta

[b] Department of Materials Science and Engineering, University of Sheffield, Sir Robert Hadfield Building, Mappin St., Sheffield, S1 3JD, UK

[c] School of Materials, University of Manchester, ICAM, Pariser Building, Manchester M13BB, UK

[d] Department of Materials Science and Engineering, Technion – Israel Institute of Technology, Haifa 32000, Israel

1. Abstract

Despite the popularity of a number of techniques of thermochemical diffusion for titanium, in many cases the surface engineering processes used may not be economically viable options for industry. This work focuses on the application of Powder Immersion Reaction Assisted Coating (PIRAC), a relatively inexpensive nitriding treatment that is capable of providing a remarkable improvement in the surface characteristics of titanium alloys. The aim of this work was to determine whether PIRAC could be successfully applied to Ti-6Al-4V and the high-performance near-α titanium alloy Timetal 834. In order to study the response of these materials to PIRAC nitriding, techniques such as X-ray diffraction, micro-indentation hardness, surface profilometry, optical and electron microscopy, nano-scratch adhesion testing and ball-on-plate reciprocating-sliding wear testing were employed. These techniques highlighted the markedly different response between the two alloys to the PIRAC treatment; namely, that Ti-6Al-4V forms a thick compound layer, while at the same processing temperature and time Timetal834 does not form any appreciable Ti_2N phase instead forming a nitrogen-diffusion case with a thin TiN compound layer at the surface. This inherent difference in nitridability influences the metallurgical response of each alloy. Despite this, the surfaces of both alloys were still hardened considerably and their tribological performance in dry sliding conditions improved compared to the untreated alloys.

2. Background and introduction

Titanium alloys are used in various industrial sectors due their advantageous properties such as a high strength-to-weight ratio, excellent corrosion resistance and maximum service temperature of up to 600 ^{o}C [1]. This generally explains their popularity in sectors such as the aerospace, chemical, medical and sports industries. However, titanium alloys suffer from poor tribological performance, which often limits their use to static structural applications. Without the use of a protective surface engineering technique, the wear rate of titanium alloys when used in sliding contact is excessively high. Additionally, the naturally occurring surface oxide film also prevents effective lubrication for wear and friction reduction.

Amongst the various thermochemical treatments used to improve the tribological performance of Ti-alloys, gas nitriding and plasma nitriding processes are the most common [2]–[7]. Nonetheless, PIRAC nitriding has been shown to provide results comparable to plasma nitriding techniques established in industry [8], [9]. Plasma nitriding typically forms thick, well-adherent compound layers with a thickness of up to 10 µm at 900 ^{o}C which drastically improves the material wear resistance [3][10]. However, complex part geometries, edges and sharp corners provide a limitation to the applicability of the process due to the formation of an "edge-effect" consisting of an area of inferior compound quality around sharp features [11][12]. On the other hand, gas nitriding processes require expensive low vacuum pumping systems in order to prevent atmospheric oxygen contamination throughout the process [2][13]. This in turn leads to a much higher capital investment required for the process compared to PIRAC nitriding where such systems are not required [8].

PIRAC nitriding is a relatively new method, having been developed in 1999 and its full investigation under dry-sliding conditions has not yet been undertaken. The PIRAC nitriding process is similar to pack cementation wherein a powder base is used to form a compound layer at the surface, however no volatile additives are used [4]. In the process the high affinity of certain reactive metals such as titanium to nitrogen, carbon, boron and silicon is harnessed for the growth of a non-oxide based ceramic compound surface layer [4]. During the process, the components to be treated are immersed in an unstable nitride powder enclosed by stainless steel foil containers containing 26 wt.% Cr. The Cr in the container walls will react with the atmospheric oxygen through the process to maintain very low oxygen pressures throughout.

Heat is applied to the containers which will result in the decomposition of the unstable nitride powders to form highly reactive monoatomic nitrogen. Reactive diffusion of the active monoatomic nitrogen in the containers results in the diffusion of the nitrogen into the near-surface region of the component forming a titanium nitride compound layer [9]. The PIRAC process and the diffusion mechanics occurring during the process are described in more detail in [8], [14]. A somewhat similar method for treating Ti-6Al-4V applied by Liu et al. as described in [15] albeit in this case the formation of TiN or Ti2N nitride compounds is intentionally supressed.

Furthermore, very little work exists on alloys other than the commonly used Ti-6Al-4V. One of the relatively recently developed high-performance near-α titanium alloys is Ti-5.8Al-4Sn-3.5Zr-0.7Nb-0.5Mo-0.35Si, also known as Timetal 834, or IMI 834. This alloy has been specifically developed for high temperature applications since it exhibits higher creep resistance and tensile strengths at elevated temperatures; above 400 ^{o}C, when compared to other titanium alloys [6]. This works aims to investigate whether the same PIRAC nitriding process can be applied to both alloys with positive results and how the processing temperature affects the alloys' surface properties. Thus, both Ti-6Al-4V and Timetal 834 (hereafter referred to as Ti64 and Ti834 respectively), were PIRAC nitrided and the resulting surface effects were studied.

3. Materials and methods

3.1.Substrate materials and PIRAC process

Cylindrical mill-annealed Ti64 and alpha-beta heat-treated Ti834 coupons of 25 mm diameter and 5 mm and 3 mm thickness respectively were prepared. The average surface roughness, R_a, of the coupons prior to treatment was 0.01 ± 0.005 μm. The chemical composition for both as-received substrates as observed using Energy Dispersive X-Ray Spectroscopy (EDX) is shown in Table 1.

Both alloys were PIRAC nitrided at 700 ^{o}C, 800 ^{o}C and 900 ^{o}C for a duration of 2 hours using the treatment methodology as described in [9], [14]. The coupons were immersed in an unstable Cr_2N nitride powder which decomposed upon heating, creating a low to moderate pressure of highly reactive mono-atomic nitrogen. The treatments took place in sealed stainless-steel foil containers containing 26 wt. % Cr. The oxygen pressure inside the container did not exceed 10^{-5} Pa. Untreated Ti-6Al-4V and Ti-5.8Al-4Sn-3.5Zr-0.7Nb-0.5Mo-0.35Si samples were used as benchmarks to the nitrided samples.

3.2. Characterisation

Glancing Incidence Asymmetric Bragg (GIAB) measurements were performed using a Rigaku Ultima IV diffractometer (CuK$_\alpha$ radiation). The measurements were made using an angle of incidence of 3°, a step size of 0.05^o and a scan speed of 0.8^o per minute in the theta range of 30° to 80°. The X-ray tube acceleration voltage was – 45 kV while the current used was 40 mA. This setup allowed for 95% of the beam intensity received at the detector to have originated from the top 1.75 µm of the material surface.

A Merlin Gemini Scanning Electron Microscope (SEM) set at an accelerating voltage of 5 kV and a probe current of 125 pA was used to observe the sample surfaces and cross-sections. The SEM was equipped with an Apollo X Ametek EDX detector used to analyse chemical composition in selected areas of interest. For the scope of this research a working distance of 15 mm with an acceleration voltage of up to – 30 kV and an electron beam current of 3 nA were used. High resolution maps of the cross-sections for samples treated at 900 ^{o}C for 2 h were taken using a rectangular grid of 50 µm by 50 µm with a step size of 150 nm for Ti64 and a rectangular grid of 100 µm by a 100 µm with a step size of 250 nm for Ti834. The different grid sizes were required due to the different grain sizes of the alloys.

Electron backscatter diffraction (EBSD) was performed using a Merlin Gemini scanning electron microscope equipped with an EBSD/EDX Ametek detector. The working distance was set to 15 mm while the working voltage and the probe current were set to 20 kV and 2 nA respectively. TSL OIM software was used to collect electron backscattered patterns for each scan. The Ti64 alloy was scanned using a rectangular grid with a grid size of 50 µm by 50 µm and a step size of 150 nm while Ti834 coupons were scanned using a grid size of a 100 µm by a 100 µm and a step size of 250 nm. Hexagonal scanning grids were used in all cases. The TSL OIM analysis software was used to automatically acquire and index the electron backscatter diffraction patterns obtained and subsequently map grain size maps of each coupon. Average grain size diameters were calculated using the method proposed by Engqvist et. al.[16].

A Veeco Dektak® 150 stylus profilometer was used to study the surface topography. The mean roughness (R$_a$) was calculated from 3 scans with a length of 1 mm taken at random positions and orientations. The diamond stylus had a tip radius of 12.5 µm and a load of 3 mg was applied together with a scan speed of 12 µm s^{-1}.

Knoop micro-indentation hardness measurements were performed using a Mitutoyo MVK-H2 micro hardness tester. Surface hardness values were taken at a load of 50 gf (1 gf = 9.81 mN) and using a 20 second dwell time. Cross-sectional hardness profiles were taken for Ti64 and Ti834 samples treated at 900 oC using a load of 25 gf with a 20 second dwell time over a depth of 100 μm.

3.3. Scratch-adhesion testing

Nanoscratch tests were performed using a Micromaterials Nanotest system equipped with a Synton-MDP 60° diamond conical indenter, with a tip radius of 5 μm. Five multi-pass scratch tests were performed using a scanning velocity of 1 μm s^{-1} over a distance of 650 μm. During the test an initial load of 0.8 mN was applied for the first 200 μm. Upon reaching 200 μm, the load was ramped up to a maximum of 450 mN at a rate of ~1 mN s^{-1}. SEM imaging and EDX line scans were used to determine the location where (and thus the indenter load at which) the substrate material was exposed.

3.4. Reciprocating-sliding wear testing

Dry-sliding wear tests were conducted using a low frequency reciprocating-sliding ball-on-plate tester. A normal load of 0.4 ± 0.01 kg (3.92 N) was applied to a stationary WC-Co (5-7 wt.%) ball with a diameter of 10 mm, having a hardness of 20.7 ± 2.2 GPa measured using Knoop micro-indentation. The applied load was selected so that the resultant maximum contact Hertzian stress (~710 MPa) in the Ti substrate would be just below its yield strength. The reciprocating frequency was set to 2 Hz with an amplitude of 7 mm and a total sliding distance of 92 m. The ambient temperature was between 24 ^{o}C and 30 ^{o}C with a relative humidity lower than 40%. Wear scar areas were measured using a Veeco Dektak 150 contact profiler.

4. Results and Discussion

4.1. Surface characterisation

After PIRAC nitriding, the substrate microstructure of both Ti alloys, shown in Figure 1, becomes visible and the surfaces gain a golden hue, which varies slightly depending on the processing temperature used. The treated coupons show no noticeable edge effects. In the case of the Ti64 alloy, typical nitride 'islands' cover the sample surface of the parent alloy while in the case of the Ti834 alloy the substrate microstructure remains clearly visible in all PIRAC

nitrided samples. Generally, for both alloys nitriding is accompanied by a distinct roughening of the surface with increasing process temperatures – reaching 0.14 µm R_a for Ti64 and 0.08 µm R_a for Ti834 at 900 ^{o}C. Compared to Ti64, the average increase in surface roughness of the Ti834 coupons is significantly lower, even at 900 ^{o}C – the highest processing temperature used.

The X-ray diffraction patterns for untreated and PIRAC nitrided Ti64 and Ti834 are shown in Figures 2 and 3 respectively. The diffractogram of the two phase Ti-6Al-4V alloy (see Figure 2) consists of several reflections corresponding to the α-Ti phase (ICDD #005-0682). However, two weak reflections corresponding to the β-phase can also be observed (ICDD #01-089-4913). Similarly, the Ti-5.8Al-4Sn-3.5Zr-0.7Nb-0.5Mo-0.35Si diffractogram (see Figure 4) consists of reflections corresponding to the α-phase and a weak β-phase (110) reflection at 38.95^o indicating a small amount of residual β-phase. An angular shift to slightly higher angles (0.15^o to 0.2^o) is present in both diffractograms obtained for untreated Ti64 and Ti834. This can be attributed to the dissolution of Al (and Sn) within the α-Ti lattice causing a shift to higher 2θ angles resulting from solid solutions and residual stresses [17], [18].

The diffraction patterns obtained following PIRAC nitrogen-diffusion treatment of Ti64 at 700 ^{o}C (shown in Figure 2), exhibit an angular shift to lower angles (approximately 0.2^o) following nitriding, indicating diffusion of interstitial nitrogen into the α-Ti lattice. EDX measurements on cross-sections of the near-surface area showed that the thickness of the nitride layer was only approximately 0.3 µm, as shown in Figure 3. No β-Ti peak can be detected following PIRAC-nitriding, as the N presence in the surface of the metal acts as a strong alpha-stabiliser. It is also evident that the GIAB technique as used in this work was not able to detect thin compound layer phases formed at 700 ^{o}C, while at 800 ^{o}C and 900 ^{o}C, nitride reflections become more apparent and intense and the nitrogen wt.% throughout the cross-sections at 800 ^{o}C and 900 ^{o}C increases accordingly. At 800 ^{o}C, reflections corresponding to ε-Ti$_2$N (ICDD #04-004-3072) appear and the reflections related to α-Ti decrease in intensity. A weak TiN(200) (ICDD #04-013-0041) reflection also appears at 42.57^o however the short process duration limits nitrogen diffusion necessary to form significant amounts of the TiN phase. Additionally, a peak at 39.7^o was observed, corresponding to the TiN$_{0.3}$ phase (ICDD #041-1352). This phase emerges by the re-organisation of nitrogen in the solid solution present in the underlying titanium substrate. As a result a non-stoichiometric nitrogen phase is formed, having a similar hexagonal crystal structure

as that of the titanium parent material [5]. Increasing the temperature to 900 ^{o}C results in an increase in intensity of the TiN and Ti$_2$N reflections coupled with a drastic decrease in the α-Ti(101) and (100) peak intensities, clearly indicating an increase in the nitride compound layer thickness. At this temperature after 2 h, the nitrogen rich Ti case together with the titanium nitride surface layers were found to be approximately 1.5 µm thick as measured using EDX maps of the near-surface area. The formation of TiN and Ti$_2$N at the surface limits the diffusion of N deeper in to the near-surface region. Furthermore, using EDX, an Al enriched zone could be observed under the surface as shown in Figure 3, likely acting as a rate determining factor for the growth of the compound layer. These two factors result in a relatively steeper, when compared to Ti834, transition from surface to bulk hardness properties as shown in Figures 3 and 5.

The Ti834 alloy responded differently to the PIRAC nitriding process compared to the Ti64 alloy. All reflections exhibit a shift by 0.4 to 0.85^{o} to lower diffraction angles, as can be observed in Figure 4. This pronounced left shift of the original Ti peaks was observed at all processing parameters and can be attributed to the interstitial diffusion of N into Ti resulting in a solid solution of nitrogen in titanium (designated here as Ti(N)). The relatively large shift in X-ray reflections to lower angles and the absence of any formation of Ti$_2$N was also reported for nitrided near-alpha alloy Ti-6Al-2Sn-4Zr-2Mo [5] while Lal et al. [19] report an exclusive formation of TiN only in nitrogen implanted Ti834. A weak reflection of TiN(200) emerges at 800 ^{o}C increasing in intensity at 900 ^{o}C and accompanied by weak reflections corresponding to TiN(111) and TiN(311) – suggesting the formation of a very thin TiN layer. The XRD technique used here revealed no detectable Ti$_2$N phase. However, a TiN compound layer of approximately 0.2 µm thickness was detected following processing at 900 ^{o}C using EDX mapping and a diffusion strengthened zone 30 µm deep together with an Al enriched zone under the compound layer were also measured (see Figure 5). The gradual transition in hardness represents a corresponding gradual transition in mechanical properties from hard nitride layer to the tough metallic substrate which has been shown to be very beneficial to the tribological performance of modified titanium surface [20].

One of the factors accounting for the difference in nitridability of the two alloys can be related to their different microstructures and grain sizes [21]. The Ti834 bimodal microstructure is less conducive to the diffusion of interstitial elements when compared to its equiaxed Ti64

counterpart. This is due to the bimodal structure's smaller grain boundary to grain volume ratio which signifies a reduced number of rapid diffusion paths [22]. The large number of rapid diffusion pathways in equiaxed alloys results in a higher diffusion rate of interstitial elements [22], hence, inherently more nitride formation. The large grain size of the Ti834 alloy (approx. 11.48 µm), when compared to the Ti64 alloy (approx. 2.26 µm), further reduces the number of grain boundaries and thus the number of diffusion pathways available for nitrogen diffusion is further decreased. The substrate microstructure thus limits the efficacy of PIRAC treatment of the Ti834 alloy resulting in a lower amount of N diffusion and therefore less formation of TiN [6]. Conversely, at higher temperatures, the barrier effect of TiN at the surface limits diffusion of N into the bulk for Ti64, while for Ti834, the absence of large amounts of TiN at the surface allows a deeper diffusion-strengthened nitrogen-rich case to form.

The Knoop hardness data obtained for the surfaces before and after PIRAC nitriding is shown in Figure 6. The untreated alloys have a hardness of 277.34 ± 9.71 kg mm^{-2} and 348.42 ± 19.88 kg mm^{-2} for Ti64 and Ti834 respectively. The slightly higher hardness of the untreated Ti834 alloy (compared to untreated Ti64) can be attributed to the alloying elements in the material; specifically Sn which is known to increase the bulk hardness of titanium by acting as a solid solution strengthener [23].

Following PIRAC nitriding, the surface hardness of both alloys increased with temperature. The Ti64 alloy exhibited a marked increase in surface hardness, while Ti834 exhibited a more modest increase after PIRAC nitriding due to the differences in the amount of nitrogen diffusion between the two alloys. In this case the indentation depth for all surfaces tested was between 0.7 and 1.15 µm and therefore the Knoop surface hardness results are mainly intended to represent the degree of load-support presented by the surface and near-surface area to resist penetration by the indenter, thus resulting in higher overall hardness measurements. Interestingly, at 700 and 800 ^{o}C the surface hardness measurements for Ti64 and Ti834 were comparable as different nitride compound layer thicknesses and N-diffusion zones roughly equated to the same degree of resistance to indenter penetration. However, for coupons nitrided at 900 ^{o}C, the relatively thick TiN/Ti$_2$N layer formed for Ti64 material resulted in a significant increase in measured surface hardness reaching 1446.46 ± 170.32 kg mm^{-2}, as opposed to the hardness of 921.58 ± 75.13 kg mm^{-2} obtained for Ti834 treated at 900 ^{o}C.

4.2. Bulk grain size analysis

The grain size of a material is known to affect mechanical properties such as the material's hardness, yield stress and fracture stress [24]. Figure 7 shows the grain size distribution maps for Ti64 and Ti834 respectively. Grains are colour coded according to the the grain diameter. Only the alpha grains were included in this analysis since (i) these constitute the vast majority of material volume and (ii) most of the beta grains in both alloys were comparable in size to the scanning step size used and this would introduce uncertainty.

Prior to treatment, the Ti64 microstructure consisted of a relatively fine equiaxed microstructure with an average diameter of 2.26 μm. The PIRAC treatment was expected to result in a small degree of grain growth partly due to the high temperatures applied. In fact, a level of grain growth was observed for all the coupons tested but the extent of grain growth varied with the different processing parameters. All PIRAC treatments carried out at 700 ^{o}C and those treated at 800 ^{o}C did not result in a large shift in the average grain size. This is evident from the similarity in the average grain diameters to that of the untreated alloy with the grain diameter increasing by 107% and 115% for the coupons treated at 700 ^{o}C and 800 ^{o}C for 2 h. With the increasing temperature, the extent of grain growth is more noticeable with treatments at 900 ^{o}C resulting in an increase in grain diameter of ~150% over the untreated substrate.

Initially, the untreated Ti834 consisted of a bimodal microstructure with an average grain diameter of 11.48 μm and no grains having diameters above 40 μm. PIRAC treatments carried out at 700 ^{o}C and 800 ^{o}C resulted in a slight increase in the average grain diameters, similar in magnitude to the increases observed for the Ti64 alloy (i.e. an increase of ~108% for this temperature range). However, unlike the case of the Ti64 alloy, the increase in average grain diameter at 900 ^{o}C for the Ti834 alloy was much more pronounced – with the mean grain diameter increasing from 11.48 μm to 28.03 μm. The increase in the volumetric average grain diameter for the coupon treated at 900 ^{o}C was of 244% over the untreated alloy. Thus, it is evident that the high temperature used in this case affected the grain size of the Ti834 alloy to a much larger extent than the Ti64 coupon treated at the same parameters.

In the untreated Ti834 alloy, the lamellae are made out of various grains separated by low and high angle grain boundaries. After PIRAC nitriding at 700 ^{o}C and 800 ^{o}C, the lamellae can still be seen to consist of amounts of smaller grains i.e. the lamellae are separated within themselves

9

by high angle grain boundaries. Treatments at 900 $^\circ$C, however, led to the coarsening of the lamellar grains, with the lamellae being made of one grain rather than a collection of alpha laths as can be seen in Figure 7. The absorption of the myriad amount of small grains and high angle grain boundaries results in the drastic increase in grain size observed. The large extent of microstructural coarsening is experienced mainly 900 $^\circ$C is very close to the heat treatment temperature used during material production leading to microstructural changes. This change in microstructure can have serious effects on the bulk mechanical performance of the alloy. Additionally, a further decrease in grain boundary volume (by the coarsening of the lamellar grains) effectively reduces the fast diffusion pathways for N even further. Therefore, during PIRAC nitriding at 900 $^\circ$C two competing effects are at play – a reduction of bulk N diffusion rate due to a decrease in grain boundary area and owing to the higher processing temperature also an increase in the driving force to diffusion.

4.3.   Tribological behaviour

The critical failure loads and indenter penetration loads for both Ti64 and Ti834 obtained in nano-scratch adhesion testing are shown in Table 2. The critical loads obtained for Ti64 exceed 300 mN; the lack of failure markers at lower loads, indicates that the nitrogen-modified surface is strongly adherent to the substrate. The high hardness of the surface compound layer contributes to the high critical loads reached before surface compound layer removal. The critical loads follow the trends observed in hardness testing as the PIRAC treatments at 900 $^\circ$C exhibit a higher critical load than the surfaces treated at 700 $^\circ$C and 800 $^\circ$C. The critical loads measured for the Ti834 coupons are all below those measured for Ti64 samples. The lower amount of nitrogen diffused into the surface, and thus the resultant lower hardness, together with the thinner compound layer formed, compared to Ti64, negatively influence the critical load required to strip the compound layer from the surface. Surprisingly, in this case, processing at 900 $^\circ$C does not result in a significant increase in critical load prior to failure. At 900 $^\circ$C, the very thin TiN surface compound formed is not as tough as the Ti_2N+TiN compound layer formed on the Ti64 coupons and therefore is not able to accommodate the plastic deformation caused during the scratch test [25]. In this case the brittle, thin TiN surface layer is unable to conform to the plastic deformation in the substrate, which results in its fracture and removal. However, the decrease in maximum depth reached (compared to coupons treated at lower

processing temperatures) suggests that the surface is able to provide an increased level of load support to the indenter, due to the higher level of N diffusion into the substrate achieved at these processing parameters, as previously discussed. The relatively large margins of error in the observed critical loads obtained for both Ti64 and Ti834 may be attributed to the localised variations in coating thickness, roughness and hardness of the treated coupons [26]. Particularly in the case of Ti834, the effect of preferential nitriding of some grain orientations cannot be dismissed. The variation in mechanical properties between the primary and secondary alpha grains can also be a factor behind the large variation in critical loads observed for Ti834 [27][28].

Figures 8 and 9 show representative images for the different scratch track morphologies observed for both Ti64 and Ti834 after PIRAC nitriding. Ductile failures were observed for all tests carried out, where the area of the exposed substrate surface was small and typically confined within the scratch track. All scratches were characterised by tensile and transverse cracks in the scratch tracks. A small amount of chipping could be seen near the end of the scratch tracks. For the rougher surfaces produced in this work, particularly Ti64 treated at 900 $^{\circ}$C, a region of asperity smoothing can be observed at the beginning of the scratch as the indenter was only in contact with the asperities as opposed to the surface (see Figure 9 (a)). For Ti834, the failure modes for surfaces subjected to treatments carried out at 900 $^{\circ}$C are very similar to those at lower temperatures; however, the fine cracks visible at lower loads (~90mN) are not present and the cracking only starts at higher loads due to the increased support provided to the indenter by the deeper N strengthened zone. The failure modes observed are typical for TiN coatings produced by diffusion processes [25].

Dry reciprocating-sliding wear tests were used to investigate the tribological characteristics of untreated Ti64, Ti834 and PIRAC nitrided surfaces. The resulting wear scar volumes for untreated Ti64 and Ti834 were measured at $15.41 \pm 0.74 \times 10^{-2}$ mm^3 and $7.49 \pm 0.49 \times 10^{-2}$ mm^3 respectively. The variations in the coefficient of friction (CoF) with sliding distance for both untreated Ti64 and Ti834 and their representative wear scar profiles are shown in Figure 10. The Ti64 surface exhibits a CoF between 0.35 to 0.4 for the first 50 m of the test, which slowly increases to 0.4 – 0.45 by the end of the test. The CoF observed for the Ti834 alloy was lower than its Ti64 counterpart with a static value of around 0.25 which increases during the test until it stabilises at around 0.35 – 0.38. The slow increase in dynamic CoF observed for both alloys can

be attributed to the transfer of Ti from the wear track to the WC-Co ball counter-face (the CoF of titanium in contact with titanium is around 0.42 to 0.47 [29][30]) – and also to the influence of wear debris which acts as third-body wear particles in the contact area [31].

The wear scars observed for both alloys appear to be similar as shown in Figure 10 (d) and (e). A large amount of plastic deformation occurred in the contact zone with the substrate material being pushed out of the scar and collecting at the edges (Figure 10 (d)). This type of wear behaviour can be attributed to severe plastic deformation of the untreated substrate coupled with severe adhesive wear due to the high reactivity of titanium when the protective and inert natural surface oxide has been removed by mechanical action [29], [32]. Scratches, abrasive grooves and some cracks normal to the sliding direction can also be observed within the scar (Figure 10 (d) and (e)). During the test cycle adhesive bonds are formed between the titanium surface and the transfer Ti layer on the WC-Co ball as the reciprocal movement proceeds. As these bonds break, they generate wear particles [32]. These particles strain harden and oxidise, which increases their hardness and in turn results in ploughing – forming the scratches observed in the wear scar (Figure 10 (d) and (e)). EDX measurements of the transfer layer observed in Figure 11 (a) and (d) confirm that the surface is in contact with a Ti transfer layer during the test, as they indicate that the material smeared on the ball surface was Ti with varying amounts of oxygen.

The shallower wear track of Ti834 (compared to Ti64) occurs as a result of the former's higher hardness and different alloying elements, specifically, its larger content of alpha stabilisers which alter the wear mechanisms occurring. These expand the titanium lattice and bring about a decrease in the resolved shear stress required for slip, resulting in a lower CoF [33], [34]. Sn is especially important; moderate Sn additions result in large lattice expansions. In fact, the addition of as little as 2.5 wt. % in literature have been observed to provide a marked reduction in CoF – indicating a decrease in the shear stress required for slip to occur [34]. Large oscillations in CoF were observed during the wear tests attributable to the presence of wear debris, resulting in third-body wear mechanisms and adhesion between the metallic titanium surface and transfer layer on the ball surface, causing stick-slip behaviour between the surface asperities. The circulation of wear particles further results in oscillations in CoF, as the friction coefficient increases when the particles accumulate and decreases when the particles are removed from the sliding contact [35]. Debris can accelerate wear by changing the two-body

sliding system into a three-body abrasion regime, which is more aggressive due to the much higher local pressures within the contact [35]. The high hardness and brittleness of the surfaces after PIRAC nitriding increase the possibility for the introduction of hard abrasive particles in the system. SEM micrographs (Figure 11 (c) and (f)) of debris collected from both Ti64 and Ti834 show mostly spherical particles having diameters of ~1 to 5 µm. Such debris is initially in the form of flakes or chips (produced by delamination) and rolled over to form spherical particles by the oscillatory motion of the test [35]. Further evidence of this is the presence of striations along the sliding direction across these platelets created by the sliding action of the ball [20]. The small number of such 'plate-like' wear particles can be related to the continuous change in sliding direction during the test, resulting in the early break-up of these plate-like particles in turn making the test mechanism more aggressive [36]. EDX analysis of wear debris collected after the test shows that this is primarily compromised of titanium (46 to 48 at.%) and oxygen (36 to 44 at.%), with some small amounts of the alloying elements. The high oxygen content in the debris can be attributed to the high contact temperatures and the debris' high surface to volume ratio as observed in [31], [37].

Wear volumes measured for Ti64 decrease drastically following PIRAC nitriding. A total wear volume of $15.41 \pm 0.74 \times 10^{-2}$ mm^3 was measured for the untreated Ti64 while, following PIRAC treatment at 700 $^{\circ}$C, the wear volume was $5.07 \pm 4.54 \times 10^{-2}$ mm^3; a reduction of approximately 67 %. In this case, the total material removal for repeated wear tests varied significantly, with some tests resulting in the removal of the hardened surface and catastrophic substrate damage, while for other test repeats, the protective nitride layer survived. Similar variations in the reciprocating sliding wear performance have been observed previously by Cassar et al. [20] for plasma nitrided Ti64 surfaces. Mainly, this can be attributed to localised variations in the compound layer properties such as thickness and hardness, combined with the overall thin hardened surface zone obtained for Ti64 at 700 $^{\circ}$C. Such a large variation in wear volumes obtained via ball-on-flat reciprocating-sliding testing is inherent to this test method [38]. Although the ball counter-face may have occasionally perforated the nitride compound layer, the resultant wear volume of the tracks where the compound layer was pierced was still persistently lower ($8.44 \pm 2.77 \times 10^{-2}$ mm^3) than that of the untreated substrate ($15.41 \pm 0.74 \times 10^{-2}$ mm^3), indicating that the PIRAC process provided a level of protection.

Increasing the PIRAC processing temperature beyond 700°C for Ti64 results in negligible wear volumes in the test conditions selected for this work. All Ti64 samples treated at 800 and 900°C survived the reciprocating tests carried out which in turn, resulted in very small measured wear volumes. The smallest wear volumes were observed for coupons nitrided at 800 °C with a measured scar volume of $1.37 \pm 0.19 \times 10^{-4}$ mm^3, and thus lower than for coupons nitrided at 900 °C ($3.14 \pm 0.42 \times 10^{-4}$ mm^3). This is particularly interesting since the latter showed superior performance in scratch adhesion testing and possessed higher surface hardness. However, PIRAC diffusion treatments at 900 °C lead to rougher surfaces which ultimately cause a higher initial wear rate − and a tendency for material pick-up, as more asperities are quickly worn off. These act as third-body wear particles and cannot easily be removed from the wear track. The formation of TiN at the surface could have also contributed to the slight increases in wear volume observed here, as TiN has been found to be more brittle than its Ti$_2$N counterpart [25] and is more abundant following PIRAC treatments at 900 °C.

A similar mechanism was observed for Ti834; after PIRAC nitriding, the wear volumes decreased significantly compared to the untreated Ti834 surfaces. However, since the hardened layer formed for this alloy is very thin, and composed predominantly of α-Ti(N) as opposed to a Ti$_2$N and/or TiN nitride compound layer, the wear tests showed significant variability in performance. This variability was not only limited to samples PIRAC treated at 700 °C but also for samples treated at 800 °C and 900 °C. A number of tests resulted in the complete removal of the hardened zone while in other (nominally identical) test runs the hardened zone was still virtually intact at the end of the test. From an initial wear volume of $7.49 \pm 0.49 \times 10^{-2}$ mm^3 observed for the untreated substrate, after PIRAC nitriding at 700 °C, a decrease in nominal wear volume was measured (with an average wear volume of $0.51 \pm 0.08 \times 10^{-2}$ mm^3); however, for around 50% of the tests the protective hardened N-rich layer was removed, resulting in substrate exposure, indicating that for these specimens the hardened zone was close to failure at the sliding distance selected for this work. Increasing the treatment temperature to 800 °C and 900 °C, improved the tribological performance of the surface, however for this alloy a number of runs resulted in catastrophic failure before the test ended and therefore the overall performance under these testing conditions can be considered inferior when compared to PIRAC-treated Ti64. The lowest nominal wear volume was obtained for coupons treated at both 800 °C ($0.77 \pm 0.522 \times 10^{-4}$ mm^3) and 900 °C ($2.22 \pm 1.52 \times 10^{-4}$ mm^3). In the case of the Ti834 surface treated at 900 °C, its superior tribological behaviour can be attributed to the deep and gradual N-diffusion profile discussed earlier, complemented with a hard − albeit thin, layer of TiN.

The inconsistency of the results obtained for PIRAC nitrided Ti834 as compared to Ti64 in reciprocating-sliding wear testing further underline the importance of the TiN/Ti_2N compound layer formation for tribological applications. A similar treatment aimed towards the formation of solely a hardened case without any TiN and Ti_2N compound formation has been investigated by Liu et al. [15] with the aim of improving the fatigue properties of titanium alloys, however, for the scope of tribological improvement of the surface the formation of solely a hardened case would not provide sufficient protection to the underlying substrate. In fact, PIRAC nitriding durations of 4 hours at temperatures of 800 ^{o}C for titanium alloys have shown that the bulk high cycle fatigue strength after treatment is mostly retained even with the formation of a thin TiN and Ti_2N compound layer at the surface of the substrate [39].

Coefficient of friction and wear mechanisms after PIRAC nitriding

Initially, all the surfaces exhibited a running in period with a very rapid increase in friction coefficient during the first 10 m of the test (as can be seen in Figures 12 and 13) – attributed to the quick generation of entrapped wear particles and the wear of the surface asperities to form a flat contact surface [40]. After the initial running-in period, the CoF stabilises. In the case of Ti64 the steady state CoF decreases from 0.41 for the untreated material to around 0.3 for PIRAC treated specimens as shown in Figure 10. For tests where failure does occur, a much higher CoF was observed combined with a large amount of oscillation in the CoF due to the abrasive action of the generated oxide and nitride particles.

For Ti834 nitrided at 700 ^{o}C, after the running-in stage the CoF value initially stabilizes at around 0.3, increasing after the removal of the hardened surface layer (indicated by the increase in CoF fluctuations) to 0.4 – 0.5, shown in Figure 11. The increase in fluctuations during the test may be attributed to the increased presence of wear debris generated after surface failure and the stick-slip behaviour of the underlying metal, with metallic substrate material transferred on the ball counterface. Before failure, the CoF values are slightly higher than those of the untreated substrate (as the surface is also rougher than the untreated surface) and after compound layer failure, the CoF values are on par with those of the untreated surface. For Ti834 surfaces treated at 800 ^{o}C and 900 ^{o}C an initial running-in stage was also observed, with the CoF reaching a steady state value of 0.38, which was maintained throughout the test.

For scars where compound layer failure has occurred, adhesive wear and some plastic deformation can be observed for both Ti64 and Ti834; Figure 12 (a). Unlike untreated Ti64, the material immediately below the compound layer is not pushed out of the wear track, suggesting a lower degree of plastic deformation of the hardened surface layer. Scratches can also be observed within the tracks, indicative of the abrasive action of wear debris (Figure 12 (a) and (b) and Figure 13 (c)). For tracks where the hardened surface was not entirely removed, an oxygen-rich transfer layer can be observed in the scratch track (Figure 12 (c, d and e). This transfer layer may have contributed to the relatively low CoF observed for these wear scars [41]. Platelets of this transfer layer were also found on the surface of the WC-Co ball counterface. The formation of an oxide transfer layer can be attributed to the high reactivity of the nitrogen –saturated solid solution zone with oxygen [41], [42]. The nitrogen-saturated solid solution zone promotes reaction with oxygen, forming an amorphous oxynitride layer leading to a low CoF and reduced adhesive wear by virtue of the low shear strength interface between the contacts [42], [43]. When this layer reaches a critical thickness, it peels off and the CoF increases rapidly. The transfer layer obtained for Ti834 samples treated at 700 ^{o}C, shown in Figure 13 (f), was found to contain ~45 at.% of oxygen. Shear-band induced cracking is present at the sides of scars obtained on Ti834, Figure 15 (d); the debris produced is comprised of fine globular particles (Figure 15 (e)). Small amounts of W were also detected in the debris indicating that some ball wear occurred.

The Ti64 nitriding processes carried out at 800 ^{o}C and 900 ^{o}C result in wear scar topographies which are very different for PIRAC treatments at 700 ^{o}C. The wear tracks of the former are nearly featureless, with evidence of smoothened asperities (Figure 16 (a, c and d)). EDX scans confirmed that N levels within the scar are similar to the unworn surface. Similarly, analysis of the ball counter face shows some transferred titanium oxide debris (Figure 16 (b)). The behaviour for Ti834 was quite different at these temperatures; coupons treated at both 800 ^{o}C and 900 ^{o}C have a (Ti-O) oxide transfer layer smeared onto the surface – as can be seen in Figure 17 (a, b and c). This transfer layer would have led to the low CoF and wear volumes observed [41]–[43]. No W was detected in the debris, indicating that wear of the ball was minimal or absent. For coupons treated at 800 ^{o}C for 2 h, the emergence of cracks along the shear bands of the grains is clearly visible (Figure 17 (d)) and tensile cracks occur in the scratch track (Figure 17 (c)). A very small amount of material was found adhered to the ball surface, compared to that observed for other processing parameters – and the debris was found to be oxidised Ti (Fig. 17 (f)). Regardless of the low amount of surface compound formation (compared to Ti64) the PIRAC process is still able to provide some level of tribological improvement to the surfaces treated under these parameters (albeit to a much lower extent than that observed on the Ti64 surfaces).

Evidently, the ball counterface did penetrate the TiN compound layer of surfaces treated at 900 ^{o}C since the depth of penetration (~0.5 µm) was more than the thickness of the TiN compound layer observed via EDX mapping. However, the TiN layer at the surface (and the limited amount of nitrogen solid solution hardening occurring beneath the layer) was still able to provide some level of support to the sliding ball by supporting its outer periphery as it penetrated into the substrate since the wear volumes obtained for the tests at 900 ^{o}C were lower than those obtained for the untreated surfaces.

5. Conclusions

The principal aim of this work was to assess and compare the ability of PIRAC nitriding to improve the tribological performance of Ti64 and Ti834 alloys. Furthermore, the effects on the surface characteristics of the two different alloys following PIRAC processing were studied.

Ti64 and Ti834 respond in markedly different ways to the PIRAC nitriding treatment. Following PIRAC processing Ti64 formed a thick compound layer, especially evident at higher processing temperatures, consisting of Ti_2N and TiN. Ti834 did not form any detectable Ti_2N phase, instead forming a nitrogen diffusion zone at the surface, covered with a thin layer of TiN. Surface hardness measurements show that an increase in surface hardness occurred after PIRAC treatment. Maximum hardnesses of 14 GPa and 8 GPa were measured for Ti64 and Ti834 respectively. Topographical measurements show that some limited surface roughening did occur at 900 ^{o}C. However, the maximum surface roughness average is still comparable to other established nitriding techniques.

The adhesion of the compound layer was measured using nano-scratch adhesion testing. Failure features such as cracking and delamination were always restricted to the scratch track. The Ti64 alloy underwent a very significant tribological improvement with considerably decreased wear volumes attributable to the thick compound layer formed following PIRAC nitriding. The tribological improvement for Ti834 was also evident, albeit to a lesser extent.

Overall, one can conclude that the PIRAC nitriding treatment, while inherently suitable for Ti64 alloys, requires tailoring if it is to maximise the tribological performance of other alloys such as Ti834. The behaviour of the two alloys when exposed to a high partial pressure of nitrogen at high temperature is dissimilar and in turn this affects the nitridability of the respective alloy.

References

[1]   M. Peters, J. Hemptenmacher, J. Kumpfert, and C. Leyens, "Structure and properties of titanium and titanium alloys," in Titanium and Titanium Alloys: Fundamentals and Applications, C. Leyens and M. Peters, Eds., 1 ed Weinheim: Wiley-VCH, 2003, pp. 1-36.

[2]   M. Nakai, M. Niinomi, T. Akahori, N. Ohtsu, H. Nishimura, H. Toda, H. Fukui, M. Ogawa , Mater. Sci. Eng. A, vol. 486, pp. 193–201, 2008.

[3]   F. Yildiz, A. F. Yetim, A. Alsaran, and A. Çelik, Surf. Coatings Technol., vol. 202, pp. 2471–2476, 2008.

[4]   E. Koyuncu, F. Kahraman, and Ö. Karadeniz, J. Achiev. Mater. Manuf. Eng., vol. 37, pp. 434–441, 2009.

[5]   A. Zhecheva, S. Malinov, and W. Sha, Surf. Coatings Technol., vol. 201, pp. 2467–2474, 2006.

[6]   T. Moskalewicz, F. Smeacetto, G. Cempura, L. C. Ajitdoss, M. Salvo, and A. Czyrska-Filemonowicz, Surf. Coatings Technol., vol. 204, pp. 3509–3516, 2010.

[7]   S. Mändl, J. W. Gerlach, and B. Rauschenbach, Surf. Coatings Technol., vol. 200, pp. 584–588, 2005.

[8]   A. Shenhar, I. Gotman, S. Radin, P. Ducheyne, and E. Y. Gutmanas, Surf. Coatings Technol., vol. 126, pp. 210–218, 2000.

[9]   A. Shenhar, I. Gotman, E. . Gutmanas, and P. Ducheyne, Mater. Sci. Eng. A, vol. 268, pp. 40–46, 1999.

[10]   S. R. Hosseini and A. Ahmadi, Vacuum, vol. 87, pp. 30–39, 2013.

[11]   D. Nolan, S. W. Huang, V. Leskovsek, and S. Braun, Surf. Coatings Technol., vol. 200, pp. 5698–5705, 2006.

[12]   E. B. Macak, W. D. Münz, and J. M. Rodenburg, J. Appl. Phys., vol. 94, pp. 2837–2844, 2003.

[13]   W. Sha, M. A. Haji Mat Don, A. Mohamed, X. Wu, B. Siliang, and A. Zhecheva, Mater. Charact., vol. 59, pp. 229–240, 2008.

[14]   E. Y. Gutmanas, I. Gotman, and W. Kaysser, Mater. Sci. Eng. A, vol. 157, pp. 233–241, 1992.

[15]   L. Liu, F. Ernst, G. M. Michal, and a. H. Heuer, Metall. Mater. Trans. A, vol. 36, pp. 2429–2434, 2005.

[16]   H. Engqvist and B. Uhrenius, Int. J. Refract. Met. Hard Mater., vol. 21, pp. 31–35, 2003.

[17]   A. C. Fernandes et al., Surf. Coatings Technol., vol. 200, pp. 6218–6224, 2006.

[18]   V. Fouquet, L. Pichon, M. Drouet, and A. Straboni, Appl. Surf. Sci., vol. 221, pp. 248–258, 2004.

[19]   A. K. Lal, S. K. Sinha, P. K. Barhai, K. G. M. Nair, S. Kalavathy, and D. C. Kothari, Surf. Coatings Technol., vol. 203, pp. 2605–2607, 2009.

[20]   G. Cassar, J. C. A. B. Wilson, S. Banfield, J. Housden, A. Matthews, and A. Leyland, Wear, vol. 269, pp. 60–70, 2010.

[21]   F. Pitt and M. Ramulu, J. Mater. Eng. Perform., vol. 13, pp. 727–734, 2004.

[22]   C. Leyens, M. Peters and W. A. Kaysser, vol. 12, pp 213-218, 1996.

[23]   M. J. Donachie, "Understanding the metallurgy of titanium," in Titanium: a Technical Guide, 2nd ed United States of America: ASM International, 2000, pp. 13-25.

[24]   A. Leyland and A. Matthews, Wear, vol. 246, pp. 1–11, 2000.

[25]   K. Farokhzadeh, A. Edrisy, G. Pigott, and P. Lidster, Wear, vol. 302, pp. 1–9, 2013.

[26]   A. J. Perry, Thin Solid Films, vol. 107, pp. 167–180, 1983.

[27]   B. Yang and H. Vehoff, Acta Mater., vol. 55, pp. 849–856, 2007.

[28]   B. S. Fromm, B. L. Adams, S. Ahmadi, and M. Knezevic, Acta Mater., vol. 57, pp. 2339–2348, 2009.

[29]   K. G. Budinski, Wear, vol. 151, pp. 203–217, 1991.

[30]   P. D. Miller and J. W. Holladay, Wear, vol. 2, pp. 133–140, 1958.

[31]   Q. Luo, Encycl. Tribol., pp. 1–11, 2013.

[32]   R. S. Magaziner, V. K. Jain, and S. Mall, Wear, vol. 267, pp. 368–373, 2009.

[33]   D. W. Wisander, NASA Tech. Note, 1976.

[34]   D. H. Buckley, T. J. Kuczkowski, and R. L. Johnson, NASA Tech. Note, 1976.

[35]   A. Zmitrowicz, vol. 43, pp. 3–35, 2005.

[36]   G. Cassar, J.C. Avelar-Batista Wilson, S, Banfield, J. Housden, M. Fenech, A. Matthews, and A. Leyland, Int. J. Fatigue, vol. 33, pp. 1313–1323, 2011.

[37]   S. Król, L. Ptacek, Z. Zalisz, and M. Hepner, J. Mater. Process. Technol., vol. 157–158, pp. 364–369, 2004.

[38]   "Standard Test Method for Linearly Reciprocating Ball-on-Flat Sliding Wear," ASTM International, Standard no. G133-5. pp. 1–9, 2005.

[39]   T. Bonello, J.C. Avelar-Batista Wilson, J. Housden, E.Y. Gutmanas, I.Gotman, A. Matthews, A. Leyland and G. Cassar, Mater. Sci. Eng. A, vol. 619, pp. 300–311, 2014.

[40]   Q. Luo, Tribol. Lett., vol. 37, pp. 529–539, 2010.

[41]   F. Pons, J. C. Pivin, and G. Farges, J. Mater. Res., vol. 2, pp. 580–587, 1987.

[42]   M. P. Kapczinski, E. J. Kinast, and C. A. Dos Santos, J. Phys. D. Appl. Phys., vol. 36, pp. 1858–1863, 2003.

[43]   D. Kakaš, P. Terek, A. Miletić, L. Kovačević, and M. Vilotić, Teh. Vjesn. - Tech. Gaz., vol. 3, pp. 27–33, 2013.

Table 1: Chemical composition in wt. % determined via EDX, balance Ti.

Element	C	O	Al	V	Fe
Ti64	0.07 ± 0.03	0.15 ± 0.05	6.4 ± 0.15	3.9 ± 0.05	0.09 ± 0.02

Element	C	O	Al	Sn	Zr	Mo	Nb	Si
Ti834	0.07 ± 0.03	0.15 ± 0.04	6.0 ± 0.2	4.1 ± 0.1	3.7 ± 0.1	0.61 ± 0.1	0.85 ± 0.15	0.6 ± 0.1

Table 2: Critical failure loads and maximum penetration depths for PIRAC nitrided Ti64 & Ti834.

Ti-Alloy	Temperature (^{o}C)	Critical load of failure (mN)	Maximum depth of penetration (μm)
Ti64	700	300.8 ± 18.2	3.6 ± 0.2
	800	318.2 ± 23.1	3.9 ± 0.1
	900	391.5 ± 30.3	3.4 ± 0.2
Ti834	700	148.0 ± 42.2	4.1 ± 0.4
	800	218.8 ± 26.1	3.6 ± 0.3
	900	210.1 ± 43.7	2.5 ± 0.4
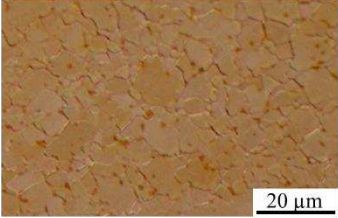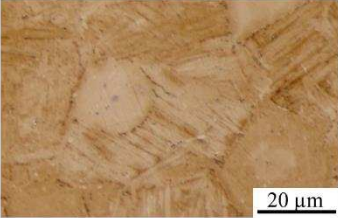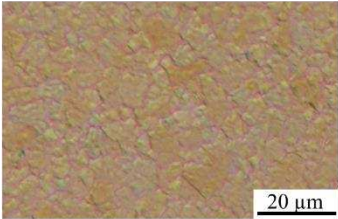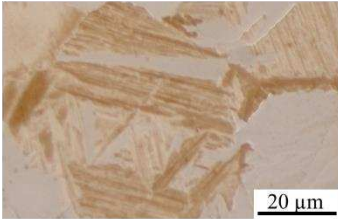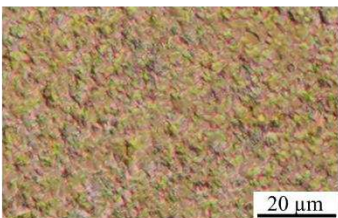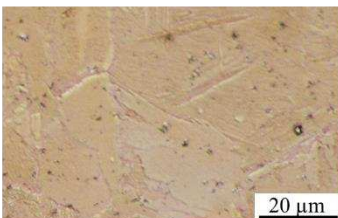
Processing Temperature	Ti64	Ti834
700 °C	R_a: 0.027 ± 0.004 μm	R_a: 0.026 ± 0.008 μm
800 °C	R_a: 0.053 ± 0.014 μm	R_a: 0.019 ± 0.005 μm
900 °C	R_a: 0.139 ± 0.003 μm	R_a: 0.084 ± 0.008 μm

Figure 1: Optical micrographs of Ti64 and Ti834 outer surfaces after PIRAC nitriding, together with their respective R_a values.
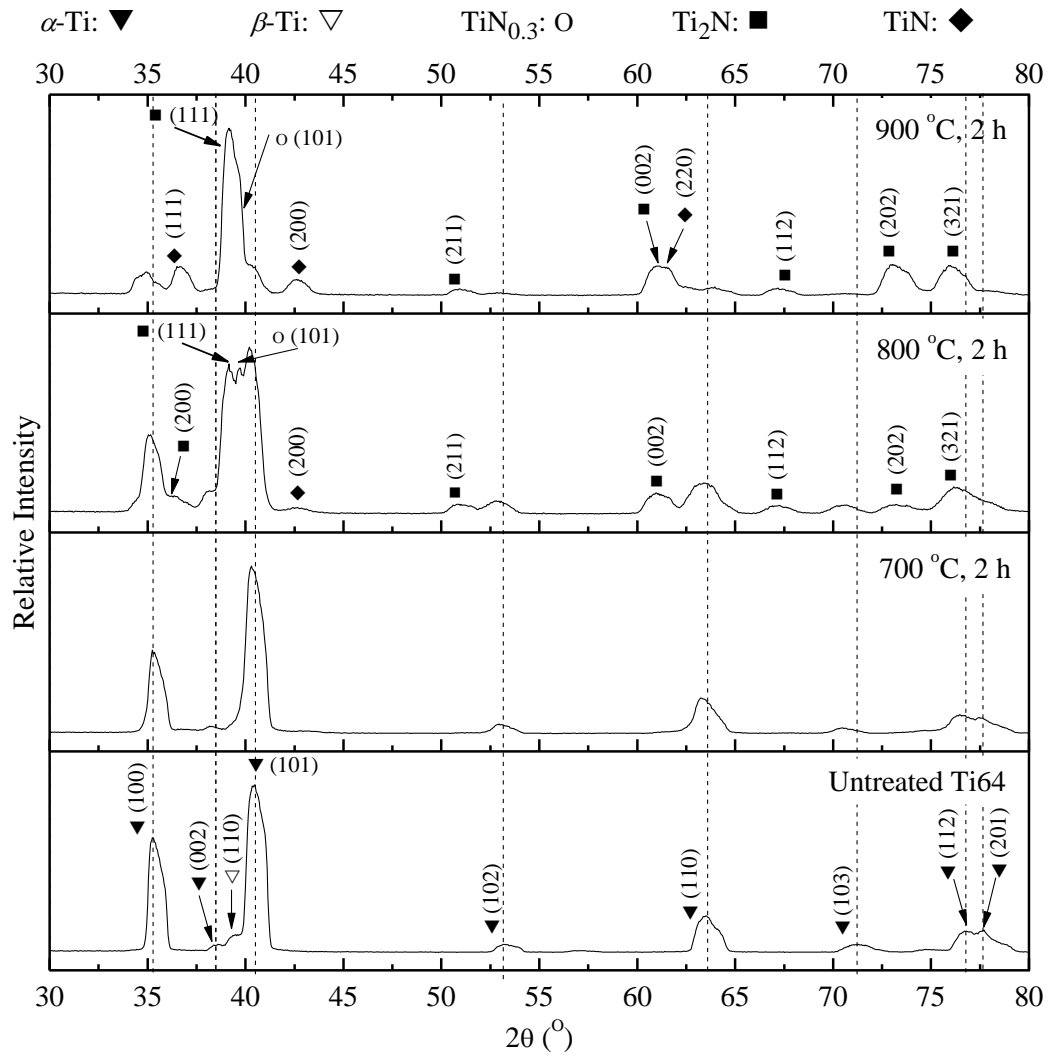
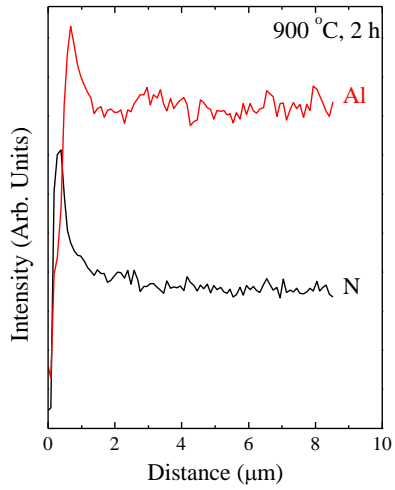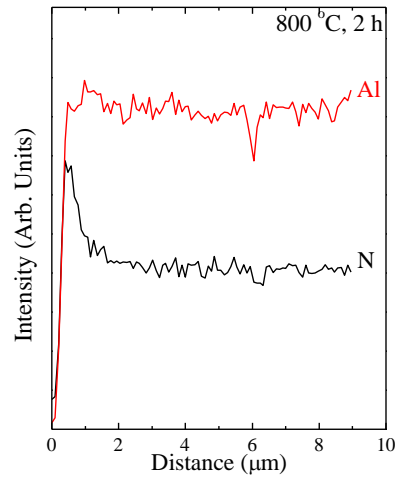**Figure 2:** X-ray diffractograms for untreated Ti64 and PIRAC nitrided Ti64.
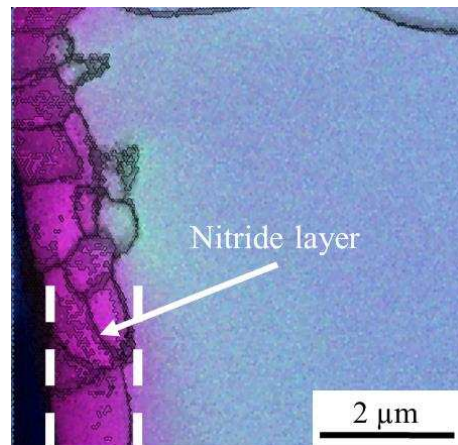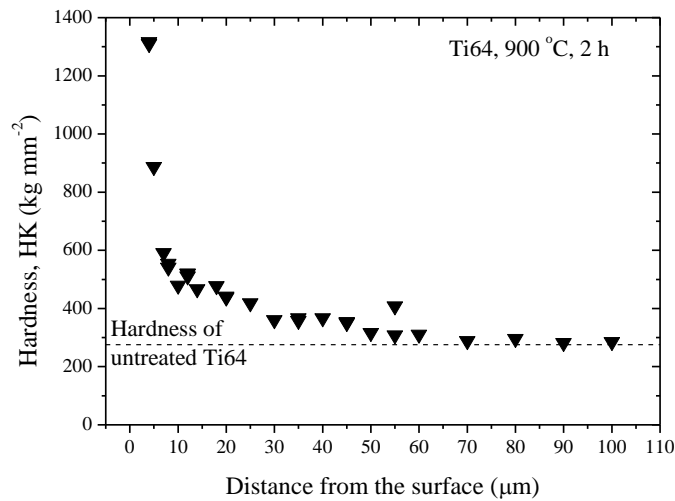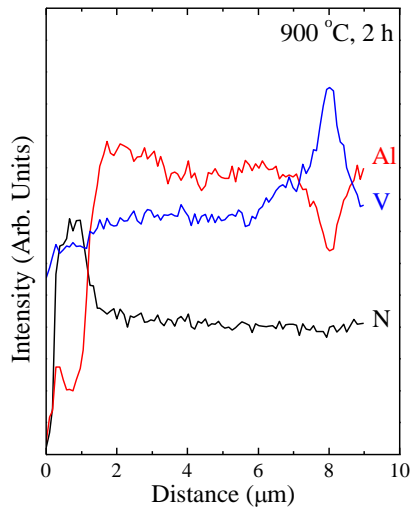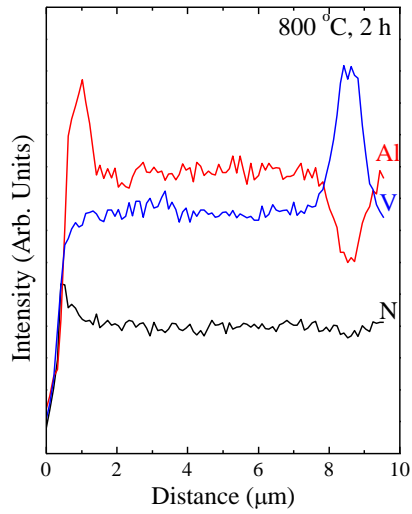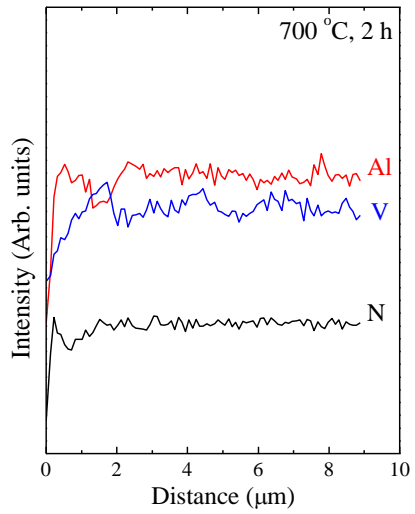
Figure 3: The chemical variation along the near-surface cross-sections for PIRAC nitrided Ti64, and a near-surface EDX map and a cross-sectional hardness plot for coupons treated at 900 °C.
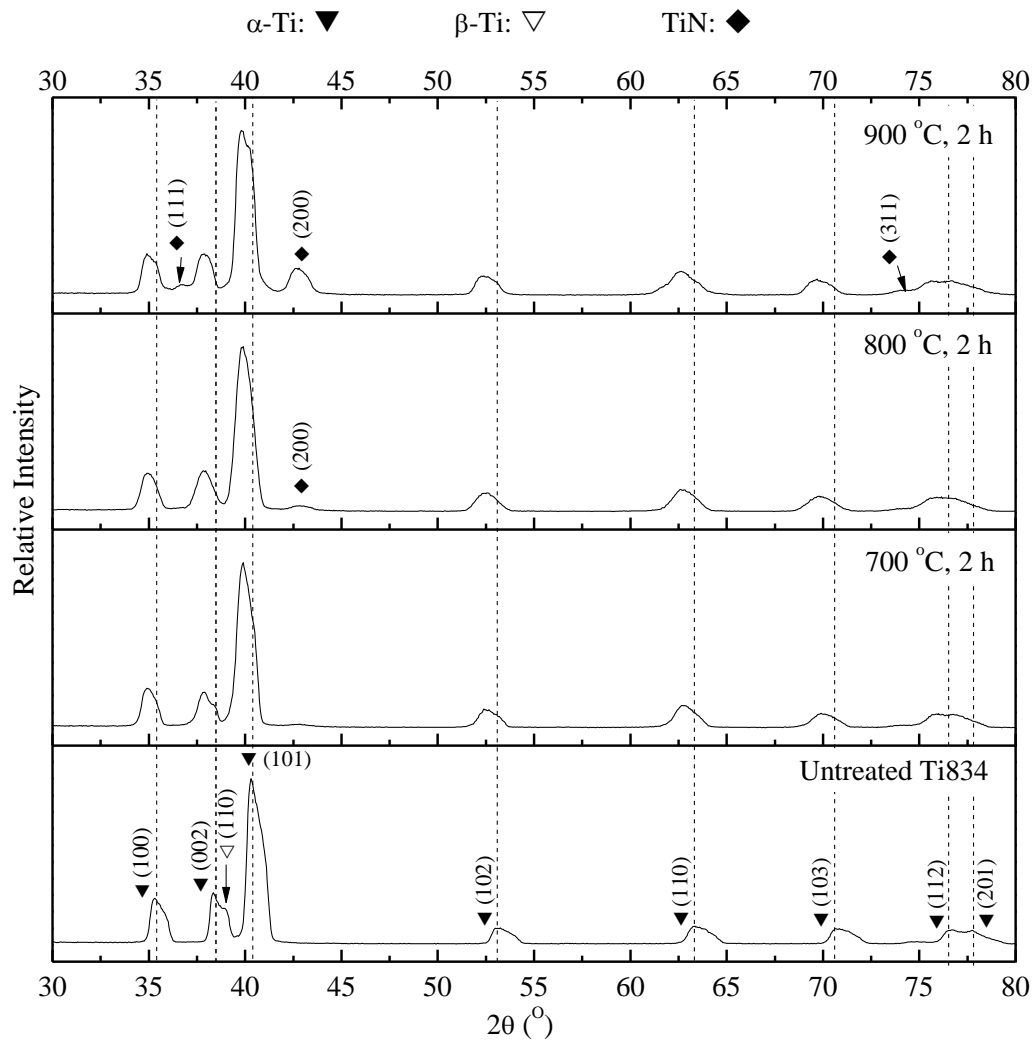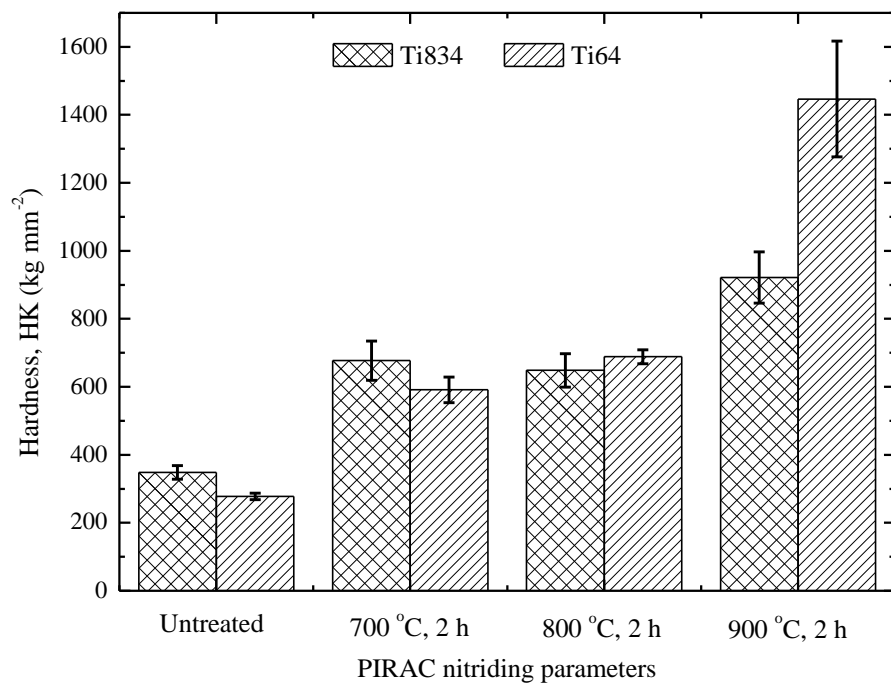
Figure 4: X-ray diffractograms for untreated Ti834 and PIRAC nitrided Ti834.
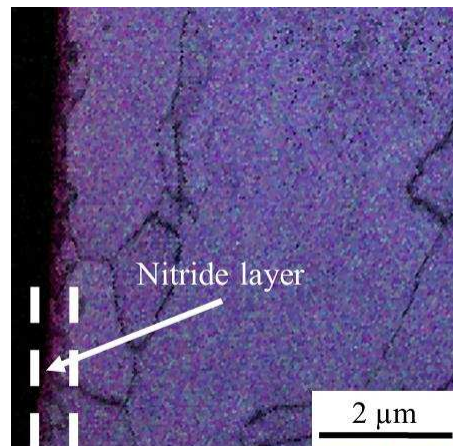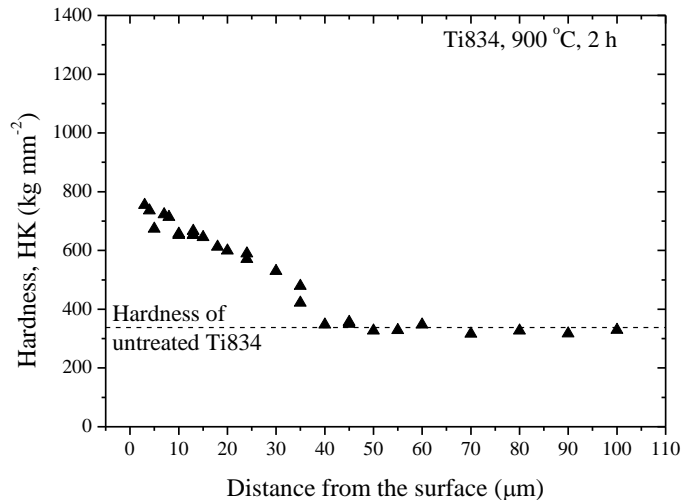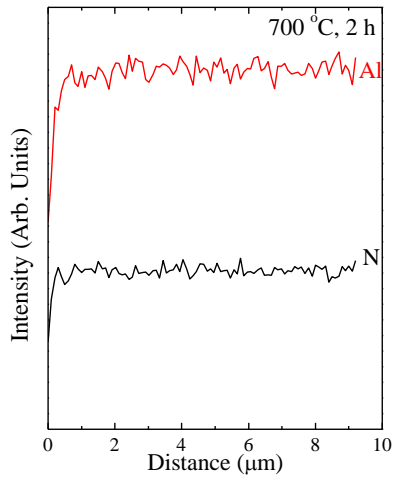
Figure 5: The chemical variation along the near-surface cross-sections for PIRAC nitrided Ti834, and a near-surface EDX map and cross-sectional hardness plot for coupons treated at 900 ^{o}C.

Figure 6: Knoop hardnesses for untreated and PIRAC nitrided Ti64 and Ti834.

Ti64	Ti834
As-received D:2.26 µm	As-received D:11.48 µm
Processing temperature: 700 °C D:2.42 µm	Processing temperature: 700 °C D:11.61 µm
Processing temperature: 800 °C D:2.62 µm	Processing temperature: 800 °C D:12.84 µm
Processing temperature: 900 °C D:3.35 µm	Processing temperature: 900 °C D:28.03 µm
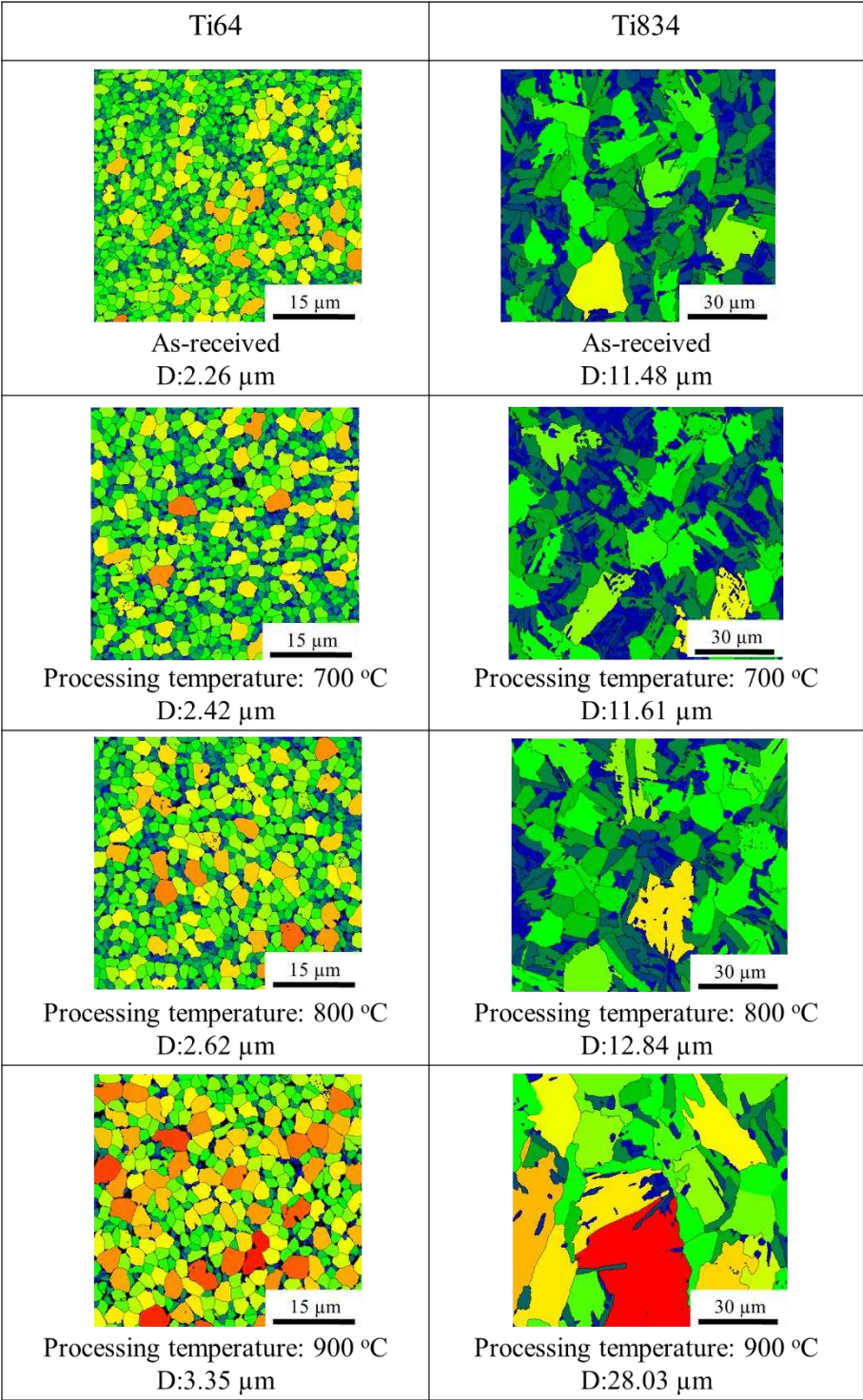
Figure 7:
EBSD grain size distribution maps for Ti64 and Ti834 before and after PIRAC treatment.
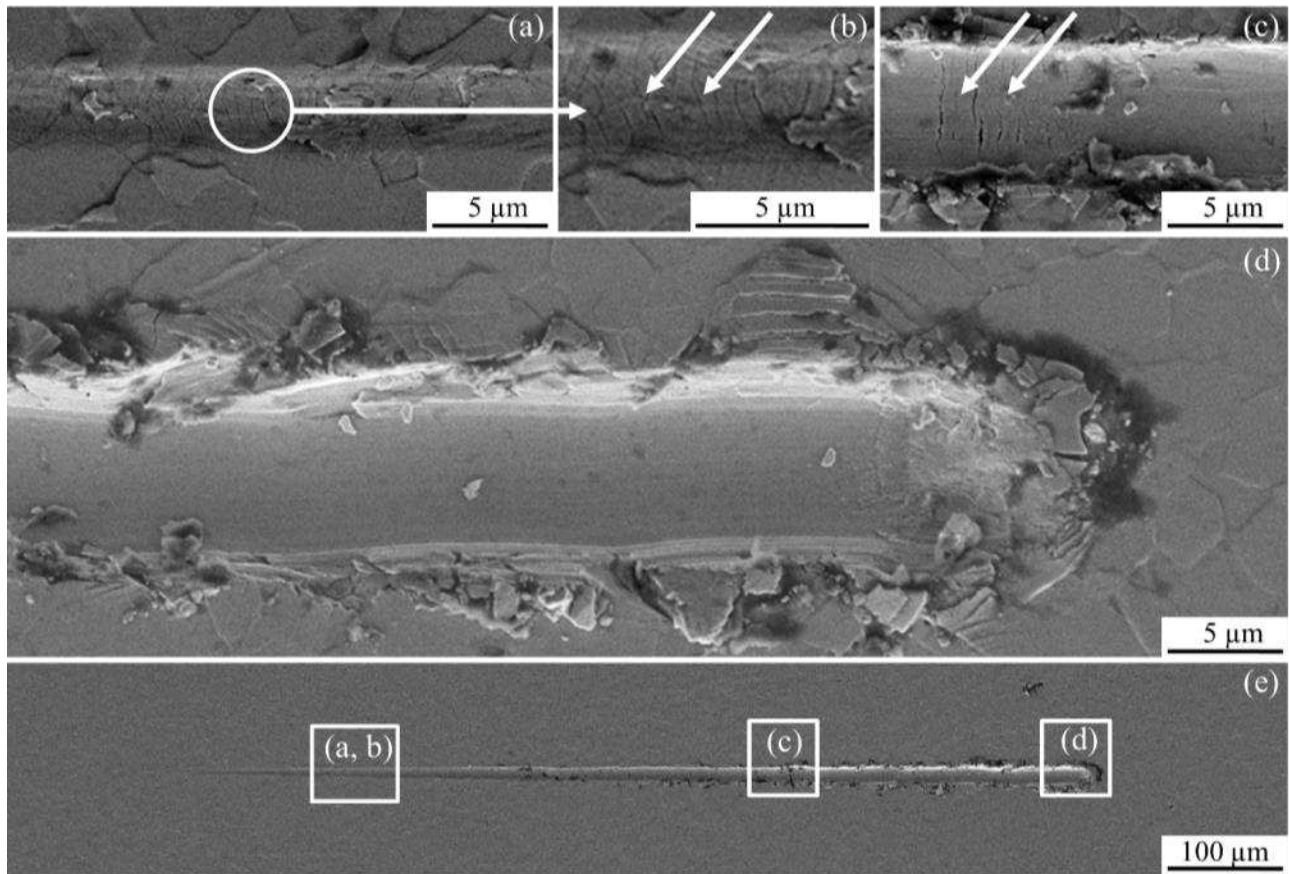
Figure 8: Representative scratch track morphologies observed for Ti64 surfaces PIRAC nitrided at 700 °C for 2 h, with (a) showing fine cracks observed in the initial part of the scratch track (below 250 mN), shown at higher magnification in (b), (c) representing the failure position, (d) the end of the scratch and (e) the complete scratch with the positions of the failure features marked. Cracking in (b and c) is marked by arrows.
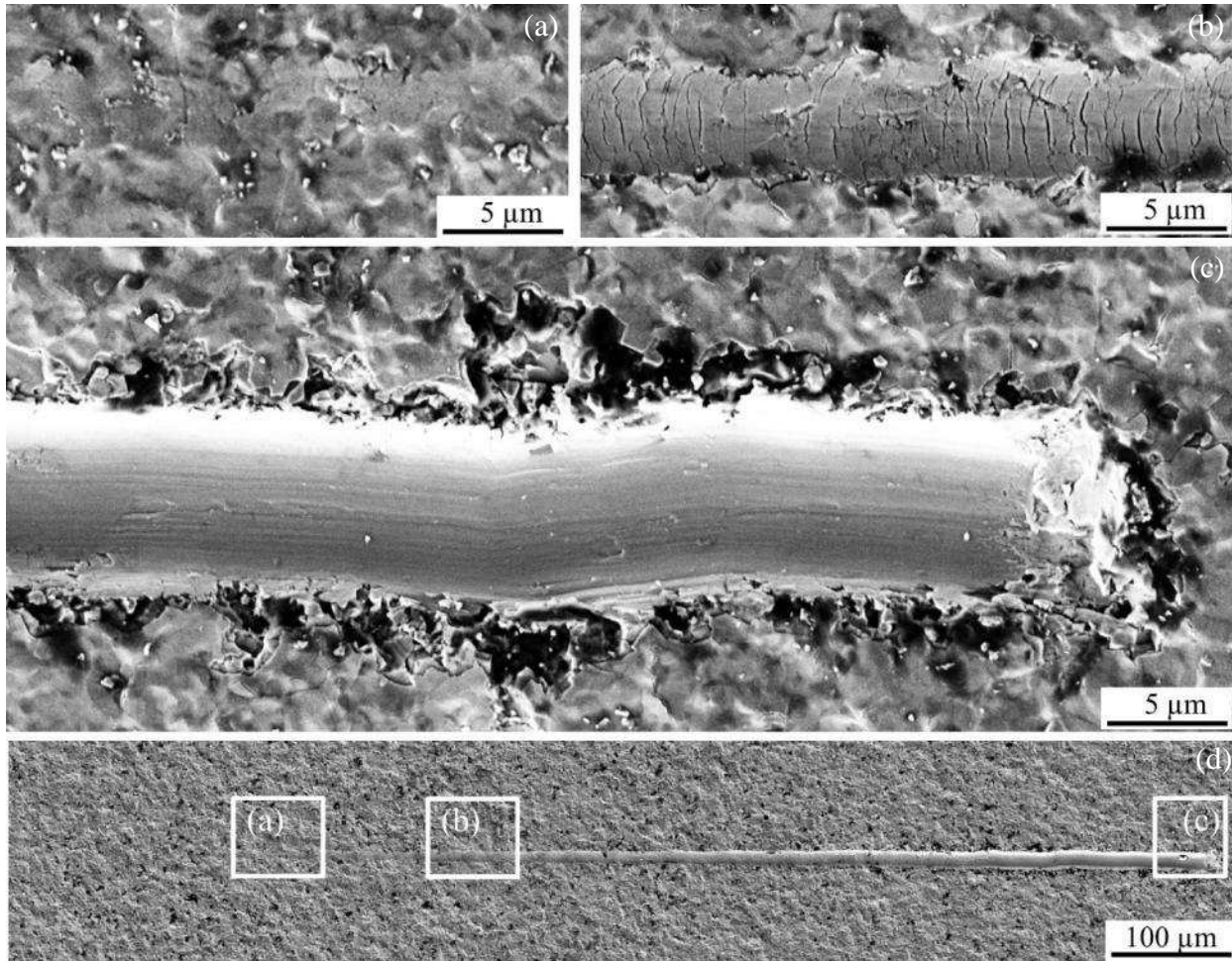
Figure 9: Representative scratch track morphologies observed for Ti64 surfaces PIRAC nitrided at 900 °C for 2 h with (a) showing the region of asperity flattening observed at the beginning of the scratch test, (b) the tensile cracks observed at bottom of the scratch track, (c) removal of the compound layer and (d) the complete scratch with the positions of the failure features marked.
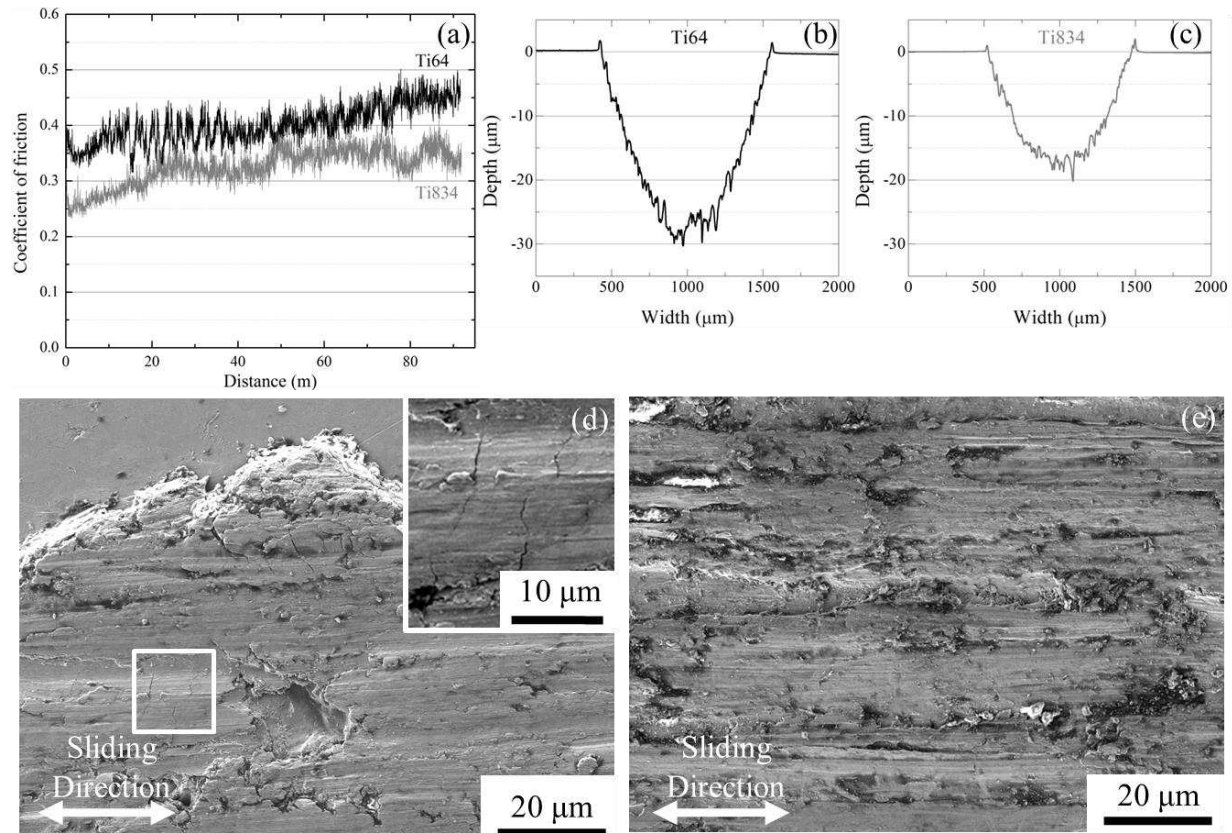
Figure 10: (a) Variation of the CoF with represeantative wear scar profiles for untreated (b) Ti64 and (c) Ti834 together with representative scar features showing (d) material pile up and cracks perpendicular to the sliding direction in the marked area for Ti64, (e) abrasive grooves and plastic deformation for Ti834.
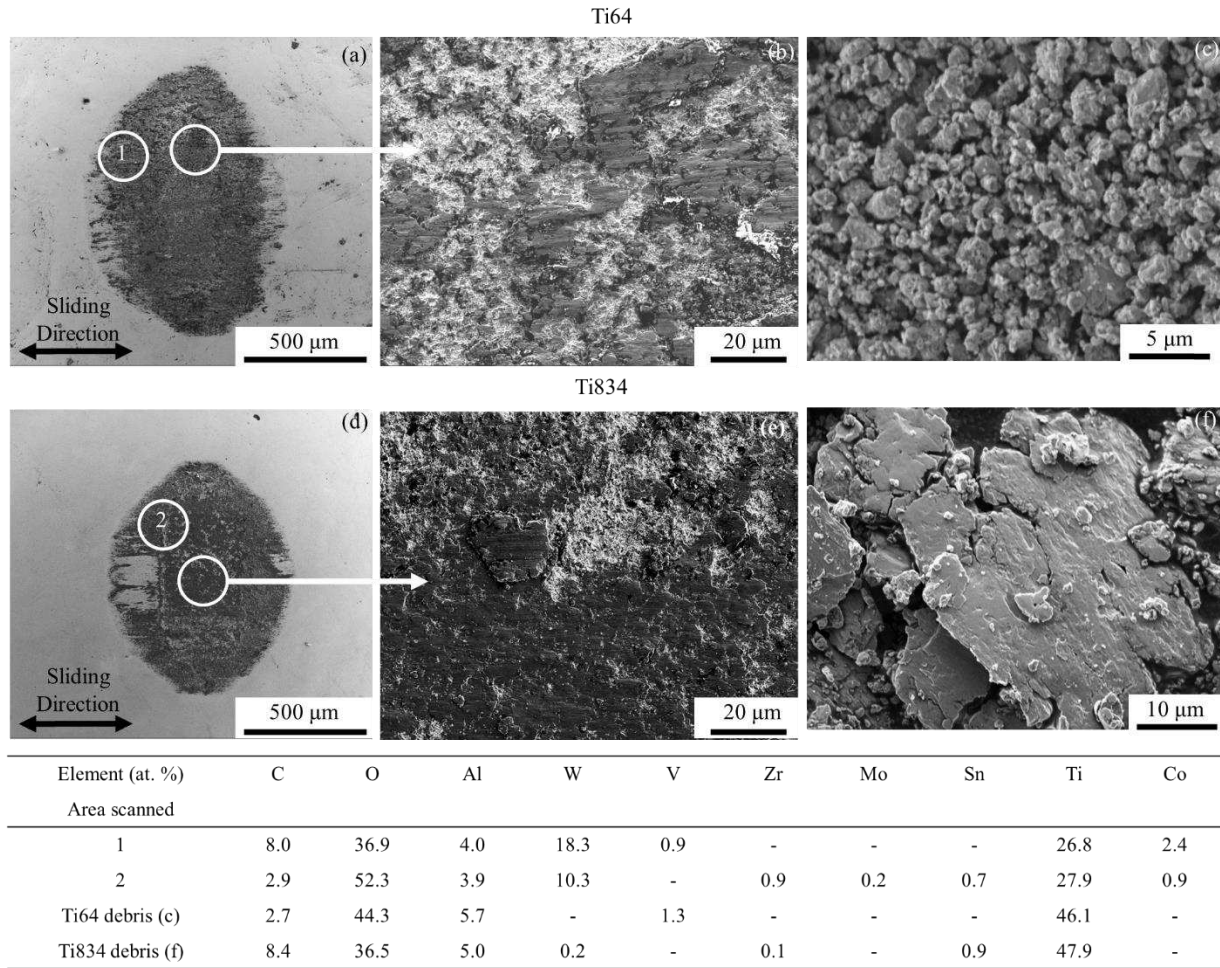
Ti64

Ti834

Element (at. %) Area scanned	C	O	Al	W	V	Zr	Mo	Sn	Ti	Co
1	8.0	36.9	4.0	18.3	0.9	-	-	-	26.8	2.4
2	2.9	52.3	3.9	10.3	-	0.9	0.2	0.7	27.9	0.9
Ti64 debris (c)	2.7	44.3	5.7	-	1.3	-	-	-	46.1	-
Ti834 debris (f)	8.4	36.5	5.0	0.2	-	0.1	-	0.9	47.9	-

Figure 11: (a and d) adhered Ti transfer layers observed on the ball surfaces, (b and e) magnified regions, (c) Ti64 agglomerated particles, (f) Ti834 plate-like debris together with the respective EDX data for the marked areas and debris.
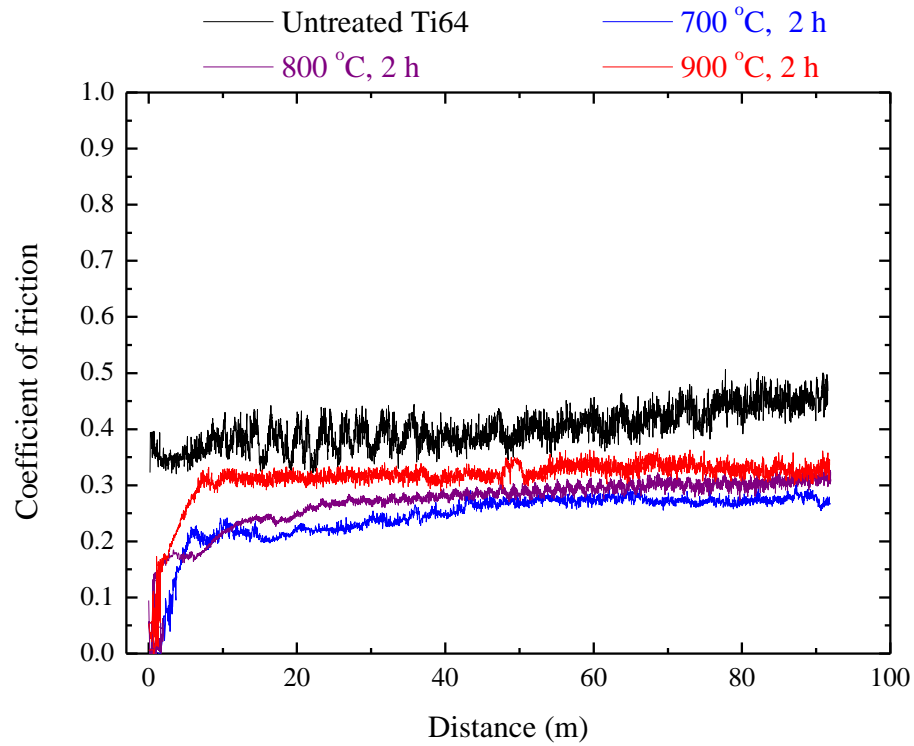
Figure 12: Representative CoF curves for untreated Ti64 and PIRAC nitrided surfaces.
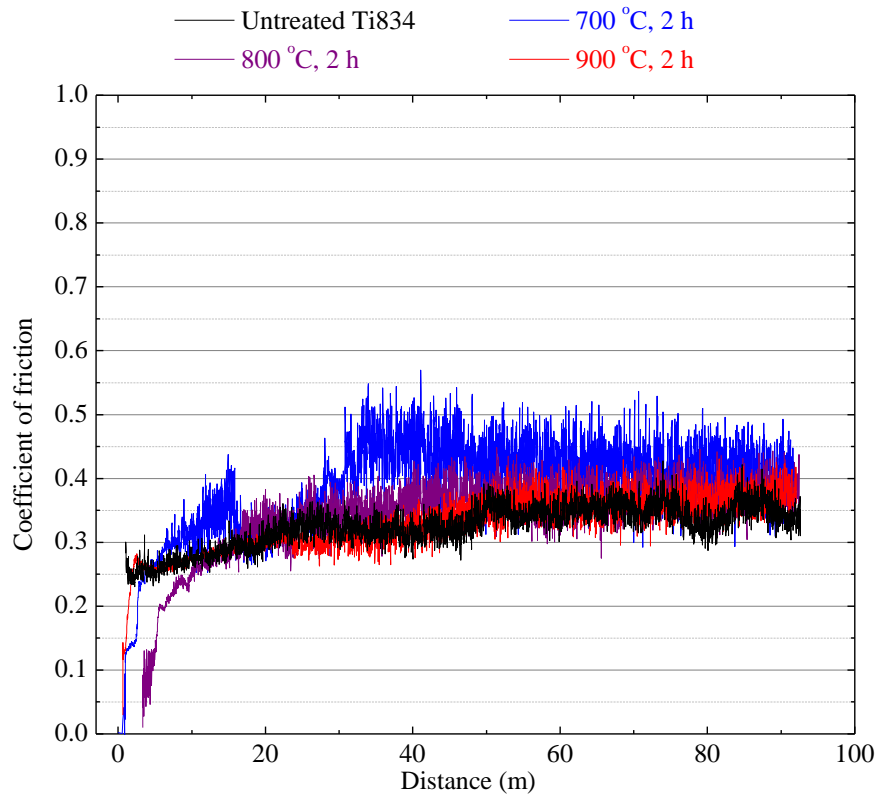
Figure 13: Representative CoF curves for untreated Ti834 and PIRAC nitrided surfaces.
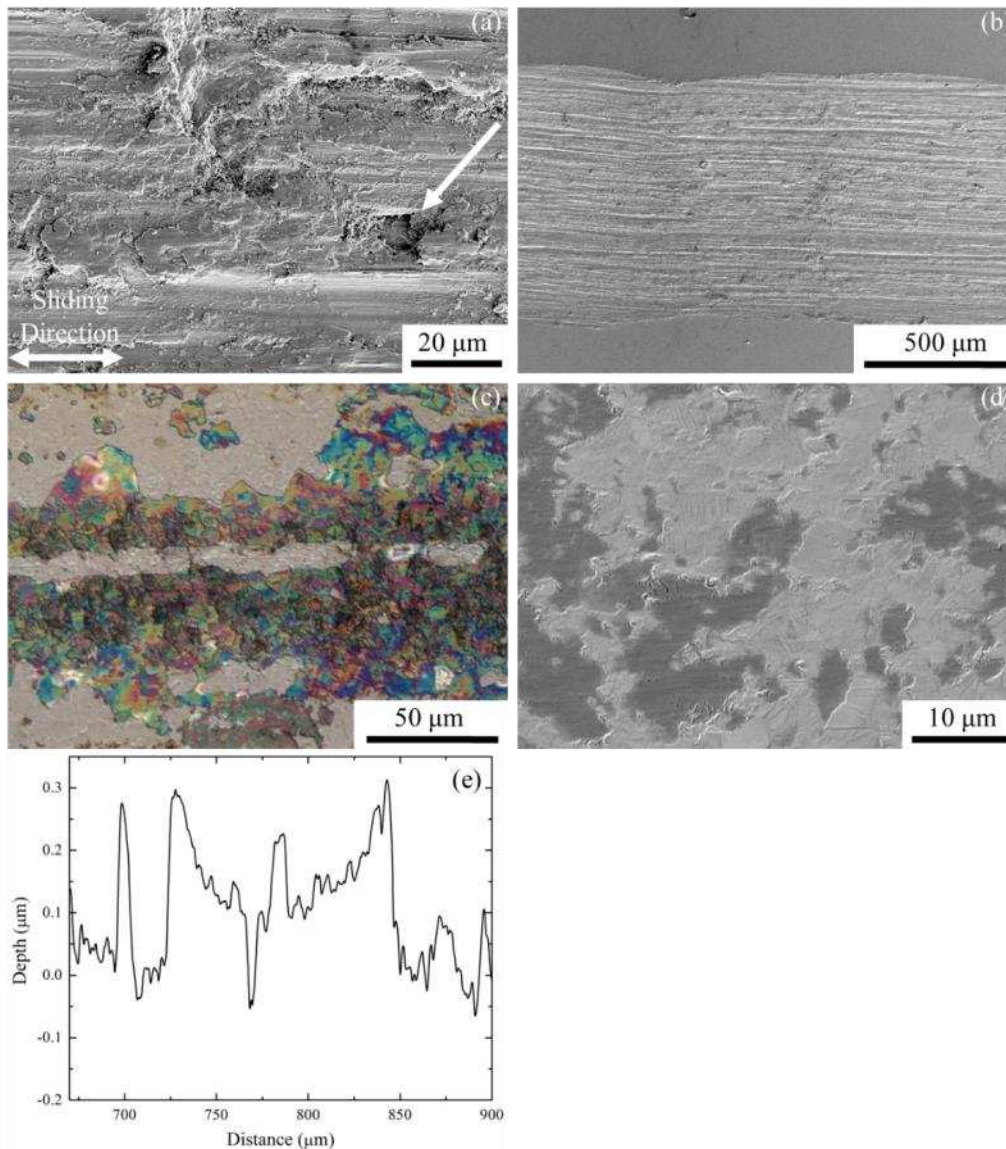
Figure 14: Micrograph of reciprocating-sliding wear tracks of Ti64 PIRAC treated at 700 °C for 2 h, where (a) shows plastic deformation and grain pull out (marked by an arrow), (b) shows lack of material push-out at the wear scar sides, (c) shows the coloration of the transfer layer, (d) the transfer layer in wear scars and (e) the profile of the transfer layer observed when the hardened surface layer was not removed.
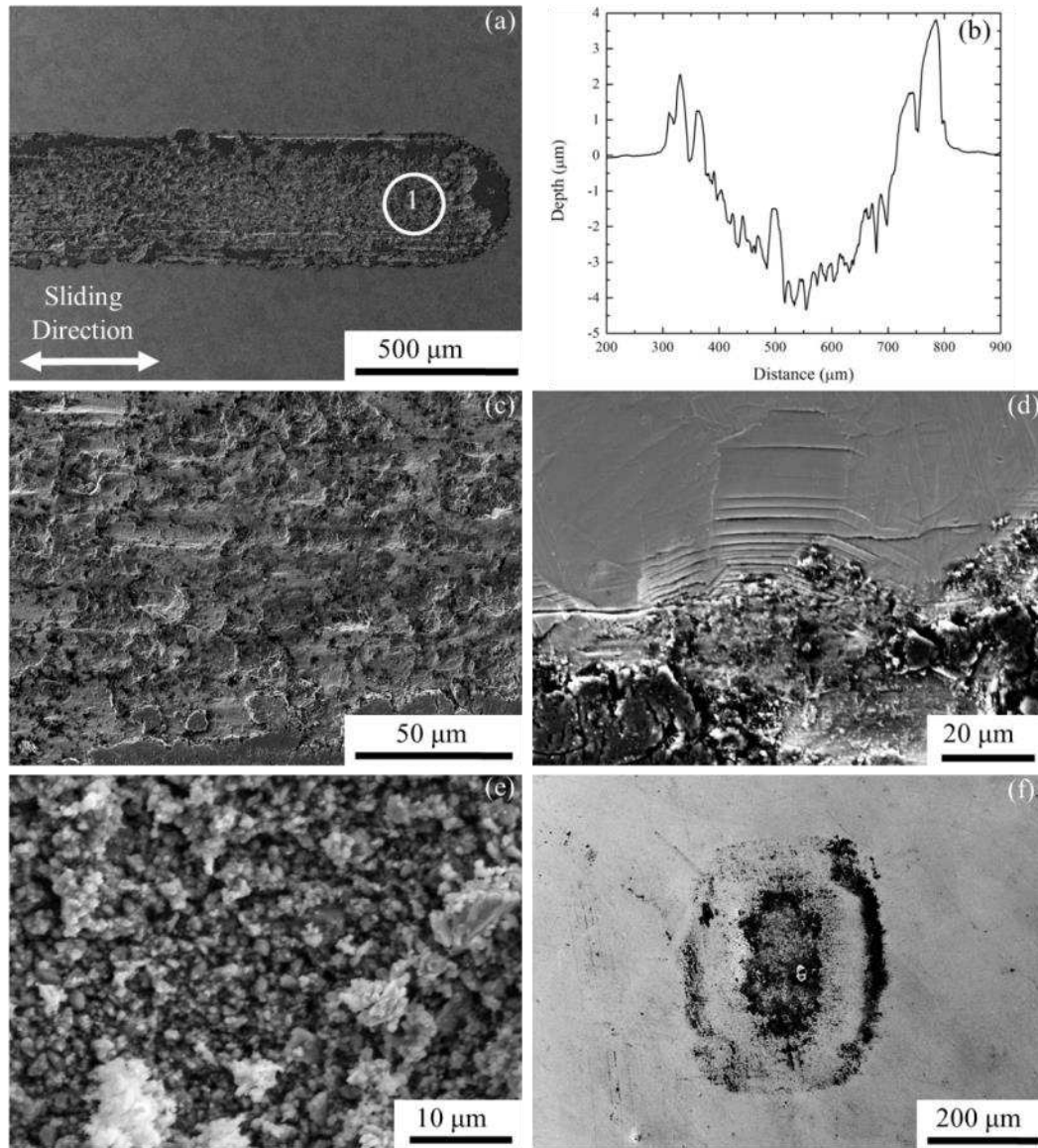
Element Area scanned	C	N	O	Al	Si	W	Zr	Nb	Sn	Ti
1 (at. %)	2.9	1.3	60.9	4.4	0.4	-	0.7	-	0.6	28.8
Debris (e) (at. %)	21.0	3.4	41.9	3.5	0.3	0.4	0.6	0.2	0.6	28.1

Figure 15: (a) Lack of material push-out from scratch, (b) wear track profile, (c) abrasion in wear track, (d) cracks along shear bands (e) wear debris, (f) transfer layer on WC-Co ball for Ti834 PIRAC nitrided at 700 ^{o}C for 2 h.
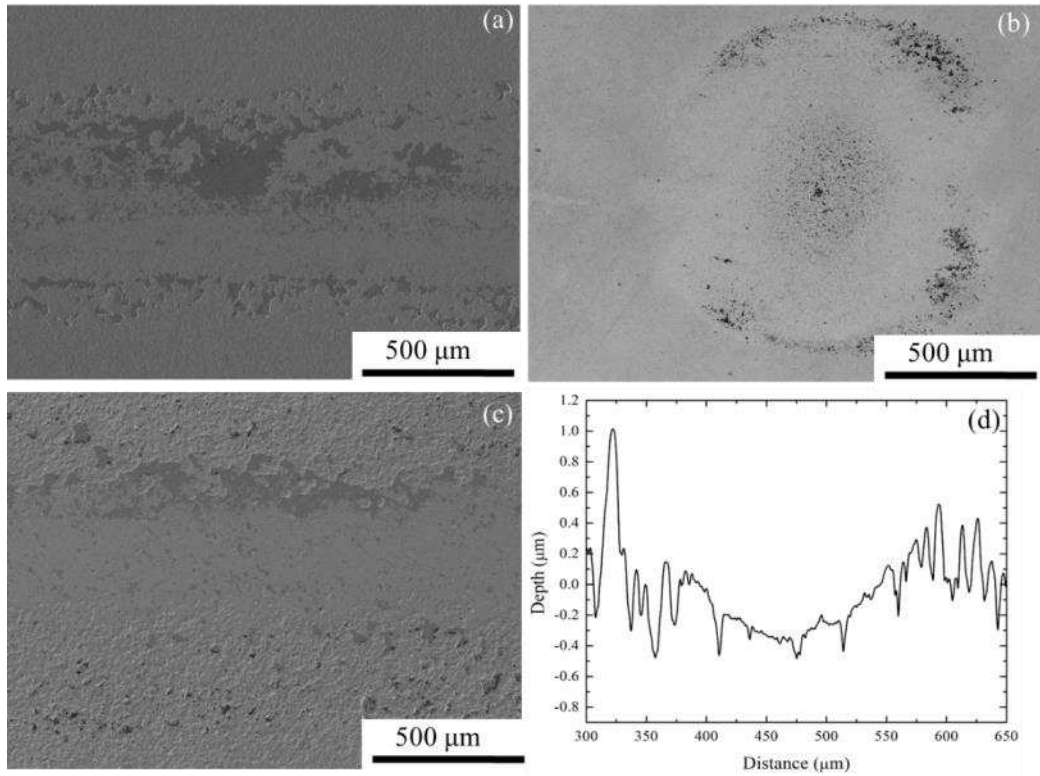
Figure 16: Wear and ball scars with (a) showing the wear scar on the disc, (b) showing a representative ball scar for Ti64 treated at 800 °C for 2 h and (c) showing the wear scar on the disc and (d) wear scar profile with asperity smoothing for Ti64 treated at 900 °C.
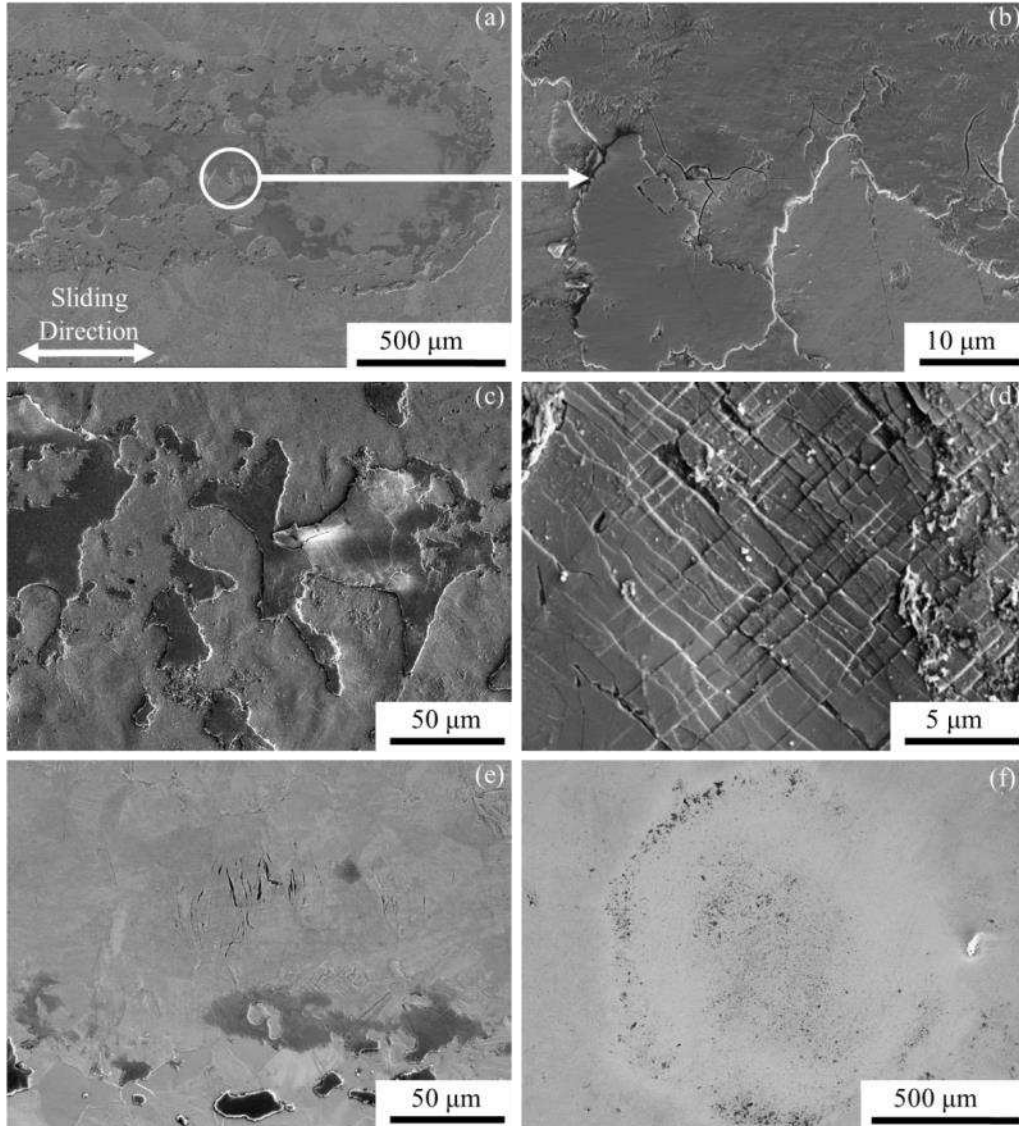
Figure 17: (a) Adhesive transfer layer and smearing observed in wear tracks for coupons PIRAC nitrided for 2 h at 900 ^{o}C shown at a higher magnification in (b), (c) adhesive transfer layer observed for treatments at 800 ^{o}C for 2 h, (d) cracking within grains, (e) tensile cracks and (f) transfer layer observed on WC-Co ball for coupons PIRAC treated at 800 ^{o}C for 2 h.